



HAL
open science

Out-of-phase Late Pleistocene glacial maxima in the Western Alps reflect past changes in North Atlantic atmospheric circulation

Natacha Gribenski, Pierre G Valla, Frank Preusser, Thibault Roattino,
Christian Crouzet, Jean-François Buoncristiani

► To cite this version:

Natacha Gribenski, Pierre G Valla, Frank Preusser, Thibault Roattino, Christian Crouzet, et al.. Out-of-phase Late Pleistocene glacial maxima in the Western Alps reflect past changes in North Atlantic atmospheric circulation. *Geology*, 2021, 49 (9), pp.1096-1101. 10.1130/G48688.1 . hal-03388270

HAL Id: hal-03388270

<https://hal.science/hal-03388270>

Submitted on 20 Oct 2021

HAL is a multi-disciplinary open access archive for the deposit and dissemination of scientific research documents, whether they are published or not. The documents may come from teaching and research institutions in France or abroad, or from public or private research centers.

L'archive ouverte pluridisciplinaire **HAL**, est destinée au dépôt et à la diffusion de documents scientifiques de niveau recherche, publiés ou non, émanant des établissements d'enseignement et de recherche français ou étrangers, des laboratoires publics ou privés.

1 **Out-of-phase Late Pleistocene glacial maxima in the Western**
2 **Alps reflect past changes in North Atlantic atmospheric**
3 **circulation**

4 **Natacha Gribenski¹, Pierre G. Valla^{2,1}, Frank Preusser³, Thibault Roattino², Christian**
5 **Crouzet², Jean-François Buoncristiani⁴**

6 *¹Institute of Geological Sciences, University of Bern, Bern, Switzerland*

7 *²ISTerre, Université Grenoble Alpes, Université Savoie Mont Blanc, CNRS, IRD, IFSTAR,*
8 *Grenoble, France*

9 *³Institute of Earth and Environmental Sciences, University of Freiburg, Freiburg, Germany*

10 *⁴UMR 6282 Biogéosciences, CNRS/Univ Bourgogne Franche-Comté, Dijon, France*

11

12

13 **ABSTRACT**

14 Paleoglacier reconstructions in the northern and southern forelands of the European Alps indicate
15 a synchronous Late Pleistocene glacial maximum during Marine Isotope Stage (MIS) 2, in phase
16 with global ice volume records. However, strong controversy remains in the western foreland,
17 where scarce and indirect dating as well as modelling studies suggest out-of-phase glacial
18 maxima with the rest of the Alps. New luminescence dating brings the first direct Late
19 Pleistocene glacial chronology for the western Alpine foreland and reveals two major glacier
20 advances of similar maximum extent, at ca. 75-60 and ca. 40-30 ka, coinciding with MIS 4 and
21 late MIS 3. We propose that asynchrony in glacial maxima between the western and the
22 northern/southern Alpine forelands results from a progressive spatial reorganization of the

23 atmospheric circulation over the North Atlantic, in response to Northern Hemisphere ice-sheet
24 fluctuations. While such feedback mechanism has emerged from general circulation models, our
25 Late Pleistocene paleoglacial reconstruction permits to track the spatio-temporal evolution of
26 moisture advection patterns over Western Europe.

27

28 **INTRODUCTION**

29 Ice-core and marine paleoclimate archives show two main periods of global temperature minima
30 during the Late Pleistocene (LP; the last ca. 130 kyr; NGRIP, 2004), coinciding with Marine
31 Isotope Stage (MIS) 4 and 2 (71-57 and 29-14 ka; Lisiecki and Raymo, 2005). Marine records
32 indicate the main peak in global ice volume, also largely reported from terrestrial glacier
33 archives, during the Last Glacial Maximum (LGM; ca. 27-19 ka; Clark et al., 2009). However,
34 local glacial maxima well before the LGM are increasingly recorded in polar and mountain
35 regions (Hughes et al., 2013; Batchelor et al., 2019). The emerging picture of variable ice
36 expansion in both time and space likely reflects the regional effect of dynamic atmospheric
37 circulations (Löfverström et al., 2014). Accurate glacial reconstructions across the globe are thus
38 crucial to constrain past atmospheric circulation and paleo-precipitation patterns (e.g.
39 Kuhlemann et al., 2008).

40 In the European Alps, major LP glaciations are recorded in prominent morainic lobes spreading
41 over several tens of kilometers in the forelands (Ehlers et al., 2011; Fig. 1). In the northern and
42 southern forelands, synchronous LP glacial maxima at ca. 26-23 ka have been documented
43 (Monegato et al., 2017). On the western side, the most extensive LP glaciation occurred in the
44 Lyon area (Fig. 1a), where an ice lobe draining the Arve (western Mont Blanc massif) and the
45 Isere catchments developed ~50 km westward into the piedmont (Coutterand et al., 2009). In
46 contrast to other Alpine forelands, scarce and indirect radiocarbon data in this area suggest older

47 LP ice-maxima than the global LGM (Mandier et al., 2003). Such asynchronous paleoglacial
48 activity is supported by numerical simulations suggesting transgressive glacier dynamics across
49 the Alps, with the observed maximum ice extent in the Western Alps only reached when
50 considering paleo-precipitation partitioning or older (i.e. MIS 4) glacier advance (Becker et al.,
51 2016; Seguinot et al., 2018).

52 To further examine the hypothesis of asynchronous paleoglacial dynamics across the Alps, a
53 robust chronology in the Western Alps is now critical. Radiocarbon and cosmogenic nuclide
54 exposure dating are challenging in this area due to the scarcity of organic material incorporated
55 within glacial deposits and in-place moraine boulders, respectively. Here, we present the first
56 direct chronology of LP ice-maximum extent in the Lyon area, using optically stimulated
57 luminescence (OSL) dating of glaciofluvial sediments. These results not only enlighten the
58 debate around the paleoglacial history of the Western Alps, but also have major implications in
59 terms of past atmospheric circulation over the North Atlantic and Western Europe.

60

61 **SETTING AND METHODS**

62 Two main moraine complexes, separated by ~25 km, define the Middle (\geq MIS 6; External
63 Moraine Complex, EMC) and Late (Internal Moraine Complex, IMC) Pleistocene ice-maximum
64 extents in the Lyon area (Buoncristiani and Campy, 2011; Fig. 1a). While the EMC presents
65 discrete, highly-degraded and discontinuous moraine crests, the IMC is characterized by a series
66 of well-defined frontal moraine ridges (Fig. 1a).

67 Glaciofluvial valleys (i.e. inactive today) expand over several tens of kilometers westward from
68 the IMC (Fig. 1a), containing large sediment infills organized in step terraces. In the western and
69 southern sectors, the IMC lays on a bedrock topographic step rising abruptly >200 m above the
70 present-day lowland (Fig. 1b). This topographic configuration allows to unambiguously relate

71 glaciofluvial sediment deposition and terraces formation to major ice-extent periods (i.e. IMC
72 ridges), when ice and meltwater could overtop this escarpment. Previous geomorphic and
73 sedimentological studies identified at least three main terrace levels which, from high (T1/T2) to
74 low (T4), directly connect to external (M2) to internal (M4) moraine ridges from the IMC
75 (Mandier, 1988; Roattino et al., 2021; Fig 1a), and thus were formed by aggradation during
76 periods of glacial advances (Marren, 2005). Typical coarse braided-river facies exposed along
77 the terraces do not permit to argue for major discontinuity in terrace construction. Discrete
78 outermost IMC ridges (M1) are visible only in the NW sector, suggesting an additional glacial
79 stage hardly preserved through subsequent glacial periods (overridden moraine patterns; Fig.
80 DR1 in the GSA Data repository), and with possible remnants in the east and south sectors of the
81 IMC indistinguishable from the M2 deposits. In the absence of direct numerical dating, it
82 remains challenging to quantitatively relate the observed glacial stages to distinct glaciations or
83 short-term glacier oscillations.

84 We targeted the three main terrace levels (T1/T2 to T4; Fig. 1a), with six samples collected from
85 well-sorted sand lenses exposed in quarry sections (Table 1, Appendix DR1). Samples were
86 taken as close as possible to the terrace surfaces to capture the last depositional period related to
87 a glacial stage. Two additional samples were collected from a glaciofluvial unit underlying till
88 from an M1 ridge in the NW sector (PIZ site; Fig. 1a, Table 1), providing maximum age
89 constraints of the LP outermost ice extent.

90 Luminescence signals and equivalent doses (D_e) were measured from quartz (green OSL) and
91 feldspar (infra-red stimulation at 50°C and 225°C, IR₅₀ and post-IRIR₂₂₅) single grains (SG, 200-
92 250 µm fraction). Methodological details are given in the GSA Data repository (DRII). Total
93 burial dose since sample deposition was determined using the Central Age Model (CAM D_e) or
94 Finite Mixture statistical model (FMM D_e) in case of partial bleaching diagnosis (Galbraith and

95 Roberts, 2012). Feldspar burial doses were corrected for anomalous fading (20-30% increase,
96 Table DR3) and final ages were calculated using sample-specific dose rate (2-3 Gy ka⁻¹ range,
97 Tables DR4,5), derived from element concentrations measured by laboratory gamma
98 spectrometry.

99

100 **RESULTS**

101 SG quartz OSL data could only be acquired for three samples (EYP1, OYT1, SPC5; Table 1), for
102 which ~2% of measured grains emit a suitable luminescence signal. This is consistent with low
103 luminescence sensitivity typically observed in quartz from crystalline bedrock and/or with
104 limited transport (Sakawuchi et al., 2011). All eight samples reveal good feldspar luminescence
105 characteristics (20-40% suitable grains).

106 SG quartz D_e distributions exhibit normal-like to moderately-skewed shapes, while SG feldspar
107 D_e distributions are widely spread, asymmetric and multimodal, with a significant fraction of
108 saturated grain for post-IRIR₂₂₅ (Figs. 2b, DR6,7). In addition, feldspar CAM D_e are significantly
109 larger (>50%) than for quartz. Both complex SG D_e distributions and CAM D_e differences
110 between feldspar and quartz are strong indicators for limited pre-depositional exposure to light,
111 typical for proximal glaciofluvial sediments (Duller, 2006). Partial bleaching, leading to age
112 overestimate, was diagnosed for most of the samples and especially for feldspar signals. We thus
113 applied statistical techniques (i.e. FMM model) to extract D_e from the best-bleached grain sub-
114 populations, giving more accurate age determination. For final age calculation, quartz OSL and
115 feldspar IR₅₀ were selected, based on their best bleaching potential.

116 Quartz OSL and feldspar IR₅₀ ages obtained from the highest terrace in the central part of the
117 study area (T1/T2: SPC5; Fig. 1a) and from the intermediate (T3: ART2, OYT1, EYP1) to lower
118 (T4: ART1) terrace levels overlap between ca. 42 and 39 ka (Fig. 3b; Table 1). Where both

119 available, quartz OSL and feldspar IR₅₀ ages agree within uncertainties, bringing further
120 confidence in the statistical treatment applied to complex feldspar IR₅₀ D_e distributions. The
121 southern highest terrace level (PEN1) resulted in a distinctly older IR₅₀ age of 63.0±11.4 ka,
122 coinciding with two IR₅₀ ages of 60.8±12.3 and 76.4±15.1 ka obtained for the glaciofluvial unit
123 underlying the north-western M1 ridge (PIZ1 and PIZ2; Table 1).

124

125 **DISCUSSION**

126 Luminescence dating indicates two periods of glaciofluvial aggradation beyond the IMC:
127 between ca. 60-75 ka and ca. 30-40 ka, coinciding with MIS 4 and late MIS 3 respectively. This
128 result strongly suggests that western Alpine glaciers reached the IMC at least twice during the
129 LP, with similar maximum ice-extent configuration. The main terrace-moraine sequence
130 (T2/T3/T4 - M2/M3/M4) observed in the area would hence result from glacier margin
131 oscillations during a single glaciation period (i.e. late MIS 3), whereas scarce and outer remnant
132 deposits (T1 - M1) were preserved from an earlier MIS 4 glacial maxima.

133 Our new MIS 4 chronology further corroborates earlier studies based on scarce chronological
134 data in the Swiss Alpine foreland (Gaar et al., 2019 and references therein), and in the nearby
135 Pyrenees (Delmas et al., 2011), as well as results from numerical simulations (Fig. 3a; Seguinot
136 et al., 2018), all of which proposed significant glaciations in the Western European mountain
137 ranges at that time. The late MIS 3 glaciation clearly predates the last glacial maxima recorded in
138 the northern and southern Alpine forelands during MIS 2 (Monegato et al., 2017). However, an
139 extended MIS 3 ice advance has been suggested in the southwestern Alpine foreland (e.g. Ivy-
140 Ochs et al., 2018), while valleys and forelands in the northern and central Alps were reported to
141 be ice-free before 30 ka (Preusser et al., 2011; Barret et al., 2017). The absence of MIS 2 ages in
142 our dataset, in particular for the lowest (T4) terrace level (ART 1, 33.8±7.3 ka), suggests that no

143 glacier advance reached the IMC after late MIS 3. This is further supported by radiocarbon ages
144 (Fig. 1a; Mandier et al., 2003) of ca. 27 to >35 ka from a paleosol above till (i.e. minimum ages)
145 in the NW sector of the IMC (Balan) and of 28-30 ka from glacio-lacustrine deposits 10-20 km
146 upstream of the IMC (Moras and Malville), which suggest shorter glacier extent in the area
147 during MIS 2. It is unlikely that the time lag (ca. 10 kyr) observed for the last major advance
148 between the Lyon and northern/southern central Alpine forelands is caused by methodological
149 uncertainties, as the applied dating approaches have shown age consistency on such timescales in
150 similar glacial settings (e.g. Smedley et al., 2016; Gribenski et al., 2018).

151 In addition to multiple and similar LP glacial maxima in the western Alpine foreland predating
152 the global LGM, our data indicates spatially and temporarily variable paleo-glacier extent
153 patterns across the European Alps, which likely reflect differential precipitation distribution
154 combined with periods of global cooling. In contrast to the modern dominance of north-west
155 atmospheric circulation, it has been proposed that south-dominated moisture advection prevailed
156 across the Alps during the LGM (Florineth and Schlüchter, 2000; Luetscher et al., 2015;
157 Monegato et al., 2017). The southward latitudinal shift of the North Atlantic storm track, as far
158 as 40°N, was forced by the development of large ice masses and sea ice in the North Hemisphere
159 (NH; Fig. 3c), as indicated by atmospheric general circulation models (e.g. Hofer et al., 2012).

160 The extensive MIS 4 glaciation in the western Alpine foreland coincides with a major cooling
161 period observed at the global and regional scales (NGRIP, 2004; Helmens, 2014; Moseley et al.,
162 2020). Further elaborating on the above circulation model, we propose that the moderate
163 expansion of the NH ice sheets during MIS 4, as indicated by deep-marine sediment records
164 (Lisiecki and Raymo, 2005), could have similarly initiated a more discrete storm-track migration
165 southward (Löffverström et al., 2014). Moisture was thus dominantly brought from the west and
166 promoted high precipitation in the west-facing massifs of the Western Alps, enabling favorable

167 conditions (i.e. wet and cold) for large piedmont glaciers. While cold MIS 4 conditions are
168 expected across the entire Alps, limited precipitation in the Central and Eastern Alps may have
169 resulted in more restricted ice extents in the main northern/southern central forelands, with
170 glacial deposits likely eroded during the greater MIS 2 extent.

171 During MIS 3, global ice records indicate a decrease of temperatures already at 40 ka before
172 reaching minima at 25-20 ka (NGRIP, 2004). Few existing long-term regional records suggest
173 similar trends in SW Europe, even with a potentially earlier cooling onset at 45 ka (Moreno et
174 al., 2014; Moseley et al., 2020). After significant shrinkage during early MIS 3, NH ice sheets
175 started to expand again from ca. 40 ka (Batchelor et al., 2019). Similar to our proposed MIS 4
176 scenario, dominant western moisture advection would have been maintained throughout mid/late
177 MIS 3 with a progressive southward shift of the polar storm track, again favoring glacier extent
178 in the Western Alps. This configuration changed with the ongoing growth of NH ice sheets
179 towards the LGM, which further pushed the polar storm track southward and lead shortly after
180 30 ka to the main southerly moisture advection over the European Alps (Luetscher et al., 2015).
181 Interestingly, the lacustrine record at Les Echets (Fig. 1a) also points towards a major change in
182 lake productivity at ca. 28-30 ka, with a climatic transition from highly-oscillating to relatively
183 stable, dry and cold conditions (Veres et al., 2009). We propose that this change in atmospheric
184 circulation resulted in significant moisture decrease over the Western Alps, while enabling
185 maximum glacier extent in the southern and northern Alpine forelands during MIS 2.

186

187 **CONCLUSIONS**

188 Our luminescence chronology constitutes the first direct evidence of two major Late Pleistocene
189 glaciations reaching similar maximum extents in the western Alpine foreland, during MIS 4 (76-
190 60 ka) and late MIS 3 (42-29 ka). These multiple and early glacial maxima revealed in the

191 western foreland contrast with MIS 2 maximum ice extent recorded in the northern and southern
192 sides of the European Alps, in phase with the global LGM. Such spatial variability in glacier
193 fluctuations has been observed elsewhere around the globe and likely translates swaying
194 atmospheric circulation and precipitation partitioning during the last glacial cycle. We propose
195 that such configuration may be related to the gradual migration of the polar storm track, forced
196 by the progressive development of NH ice sheets. This study further highlights the importance of
197 regional paleo-glacier reconstructions and numerical chronologies for quantifying past changes
198 in atmospheric circulation patterns.

199

200 **ACKNOWLEDGMENTS**

201 This work was supported by the SNSF (PP00P2_170559), INSU and USMB (AAP Montagne).
202 We thank Gachet TP, Eiffage, Cemex Granulat Rhône Méditerranée, Nord Isère Matériaux and
203 Vicat Granulat for providing access to gravel pits. We thank the four anonymous reviewers for
204 their valuable suggestions.

205

206

207 **REFERENCES**

208 Barrett, S.J., Starnberger, R., Tjallingii, R., Brauer, A., and Spötl, C., 2017, The sedimentary
209 history of the inner-alpine Inn Valley (Austria): extending the Baumkirchen type section
210 further back in time with new drilling: *Journal of Quaternary Science*, v. 32, p. 63–79,
211 <https://doi.org/10.1002/jqs.2924>
212 Batchelor, C.L., Margold, M., Krapp, M., Murton, D.K., Dalton, A.S., Stokes, C.R., Murton,
213 J.B., and Manica, A., 2019, The configuration of Northern Hemisphere ice sheets through

214 the Quaternary: Nature Communications, v. 10, p. 3713, <https://doi.org/10.1038/s41467->
215 019-11601-2

216 Becker, P., Seguinot, J., Jouvét, G., and Funk, M., 2016, Last Glacial Maximum precipitation
217 pattern in the Alps inferred from glacier modelling: *Geographica Helvetica*, v. 71, p.
218 173–187, <https://doi.org/10.5194/gh-71-173-2016>

219 Buoncristiani, J.-F. and Campy, M., 2011, Quaternary glaciations in the French Alps and Jura:
220 Developments in Quaternary Sciences, v. 15, p. 117–126, <https://doi.org/10.1016/B978->
221 0-444-53447-7.00010-6

222 Clark, P.U., Dyke, A.S., Shakun, J.D., Carlson, A.E., Clark, J., Wohlfarth, B., Mitrovica, J.X.,
223 Hostetler, S.W. and McCabe, A.M., 2009, The Last Glacial Maximum: *Science*, v. 325,
224 p. 710–714, <https://doi.org/10.1126/science.1172873>

225 Coutterand, S., Schoeneich, P., Nicoud, G., 2009, Le lobe glaciaire lyonnais au maximum
226 würmien : glacier du Rhône ou/et glaciers savoyard?. Philip Deline, Ludovic Ravel. *Neige et glace de montagne : Reconstitution, dynamique, pratiques*, Collection EDYTEM
227 - Cahiers de Géographie, v. 8, p. 11–22, <halshs-00389085>

229 Delmas, M., Calvet, M., Gunnell, Y., Braucher, and R., Bourlès, D., 2011, Paleogeography and
230 ¹⁰Be exposure-age chronology of Middle and Late Pleistocene glacier systems in the
231 northern Pyrenees: implications for reconstructing regional paleoclimates:
232 *Palaeogeography, Palaeoclimatology, Palaeoecology*, v. 305, p.109–122,
233 <https://doi.org/10.1016/j.palaeo.2011.02.025>

234 Duller, G.A.T., 2006, Single grain optical dating of glacial deposits: *Quaternary*
235 *Geochronology*, v. 1, p. 296–304, <https://doi.org/10.1016/j.quageo.2006.05.018>

236 Ehlers, J., Gibbard, P.L., and Hughes, P.D., eds., 2011, Quaternary Glaciations - Extent and
237 Chronology: A Closer Look: Developments in Quaternary Science, v. 15. Elsevier,
238 Amsterdam, 1108 p.

239 Florineth, D., and Schlüchter, C., 2000, Alpine evidence for atmospheric circulation patterns in
240 Europe during the Last Glacial Maximum: Quaternary Research, v. 54, p. 295–308,
241 <https://doi.org/10.1006/qres.2000.2169>

242 Gaar, D., Graf, H.R., and Preusser, F., 2019, New chronological constraints on the timing of Late
243 Pleistocene glacier advances in northern Switzerland, E & G Quaternary Science Journal,
244 v. 68, p. 53–73, <https://doi.org/10.5194/egqsj-68-53-2019>

245 Galbraith, R.F., and Roberts, R.G., 2012, Statistical aspects of equivalent dose and error
246 calculation and display in OSL dating: An overview and some recommendations:
247 Quaternary Geochronology, v. 11, p.1–27, <https://doi.org/10.1016/j.quageo.2012.04.020>

248 Gribenski, N., Jansson, K.N., Preusser, F., Harbor, J.M., Stroeven, A.P., Trauerstein, M.,
249 Blomdin, R., Heyman, J., Caffee, M.W., Lifton, N., and Zhang, W., 2018, Re-evaluation
250 of MIS 3 glaciation using cosmogenic radionuclide and single grain luminescence ages,
251 Kanas Valley, Chinese Altai: Journal of Quaternary Science, v. 33, p. 55–67,
252 <https://doi.org/10.1002/jqs.2998>

253 Helmens, K.F., 2014, The Last Interglacial Glacial cycle (MIS 5-2) re-examined based on long
254 proxy records from central and northern Europe: Quaternary Science Reviews, v. 86, p.
255 115–143, <http://dx.doi.org/10.1016/j.quascirev.2013.12.012>

256 Hofer, D., Raible, C.C., Merz, N., Dehnert, A., and Kuhlemann, J., 2012, Simulated winter
257 circulation types in the North Atlantic and European region for preindustrial and glacial
258 conditions: Geophysical Research Letters, v. 39, L15805,
259 <http://dx.doi.org/10.1029/2012GL052296>

260 Hughes, P.D., Gibbard, P.L., Ehlers, J., 2013, Timing of glaciation during the last glacial cycle:
261 evaluating the concept of a global ‘Last Glacial Maximum’ (LGM): *Earth-Science*
262 *Reviews*, v. 125, p. 171–198, <https://doi.org/10.1016/j.earscirev.2013.07.003>

263 Ivy-Ochs, S., Lucchesi, S., Baggio, P., Fioraso, G., Gianotti, F., Monegati, G., Graf, A.A., Akçar,
264 N., Christl, M., Carraro, F., Gabrialla Forno, M., and Schlüchter, C., 2018, New
265 geomorphological and chronological constraints for glacial deposits in the Rivoli
266 Avigliana end-moraine system and the lower Susa Valley (Western Alps, NW Italy):
267 *Journal of Quaternary Science*, v. 33, p. 550–562, <https://doi.org/10.1002/jqs.3034>

268 Kuhlemann, J., Rohling, E.J., Krumrei, I., Kubik, P., Ivy-Ochs, S. and Kucera, M., 2008,
269 Regional synthesis of Mediterranean atmospheric circulation during the Last Glacial
270 Maximum: *Science*, v. 321, p. 1338–1340, <https://doi.org/10.1126/science.1157638>

271 Lisiecki, L.E. and Raymo, M.E., 2005, A Pliocene-Pleistocene stack of 57 globally distributed
272 benthic ¹⁸O records: *Paleoceanography*, v. 20, p. 1–17,
273 <https://doi.org/10.1029/2004PA001071>

274 Löffverström, M., Caballero, R., Nilsson, J., and Kleman, J., 2014, Evolution of the large-scale
275 atmospheric circulation in response to changing ice sheets over the last glacial cycle:
276 *Climate of the Past*, v. 10, p. 1453–1471, <https://doi.org/10.5194/cp-10-1453-2014>

277 Luetscher, M., Boch, R., Sodemann, H., Spötl, C., Cheng, H., Edwards, R. L., Frisia, S., Hof, F.,
278 and Müller, W., 2015, North Atlantic storm track changes during the Last Glacial
279 Maximum recorded by Alpine speleothems: *Nature Communications*, v. 6, p. 6344,
280 <https://doi.org/10.1038/ncomms7344>

281 Mandier, P., 1988, *Le relief de la moyenne vallée du Rhône au Tertiaire et au Quaternaire: essai*
282 *de synthèse paléogéographique*. Bureau de Recherches Géologiques et Minières, Orléans,
283 865 pp.

284 Mandier, P., Evin, J., Argant, J., and Petiot, R., 2003, Chronostratigraphie des accumulations
285 würmiennes dans la moyenne vallée du Rhône. L'apport des dates radiocarbone:
286 Quaternaire, v. 14/2, p. 113–127, <https://doi.org/10.3406/quate.2003.1735>

287 Marren, P., 2005, Magnitude and frequency in proglacial rivers: a geomorphological and
288 sedimentological perspective: *Earth Science Reviews*, v. 70, p. 203–251,
289 <https://doi.org/10.1016/j.earscirev.2004.12.002>

290 Moreno, A., Svensson, A., Brooks, S.J., Connor, S., Engels, S., Fletcher, W., Genty, D., Heiri,
291 O., Labuhn, I., Persiou, A., Peyron, O., Sadori, L., Valero-Garces, B., Wulf, S., and
292 Zanchetta, G., 2014, A compilation of Western European terrestrial records 60-8 ka BP:
293 towards an understanding of latitudinal climatic gradients: *Quaternary Science Reviews*,
294 v. 106, p. 167–185. <https://doi.org/10.1016/j.quascirev.2014.06.030>

295 Monegato, G., Scardia, G., Hajdas, I., Rizzini, F., and Piccin, A., 2017, The Alpine LGM in the
296 boreal ice-sheets game: *Nature Scientific reports*, v. 7, p. 2078,
297 <https://doi.org/10.1038/s41598-017-02148-7>

298 Moseley, G.E., Spötl, C., Brandstätter, S., Erhardt, T., Luetscher, M., and Edwards, R.L., 2020,
299 NALPS19: sub-orbital-scale climate variability recorded in northern Alpine speleothems
300 during the last glacial period: *Climate of the Past*, v. 16, p. 29–50,
301 <https://doi.org/10.5194/cp-16-29-2020>

302 NGRIP members, 2004, High-resolution record of Northern Hemisphere climate extending into
303 the last interglacial period: *Nature*, v. 43, p. 147–151,
304 <https://doi.org/10.1038/nature02805>

305 Preusser, F., Graf, H. R., Keller, O., Krayss, E., and Schlüchter, C., 2011, Quaternary glaciation
306 history of northern Switzerland: *E&G Quaternary Science Journal*, v. 60, p. 21,
307 <https://doi.org/10.3285/eg.60.2-3.06>

- 308 Roattino, T., Crouzet, C., Buoncristiani, J-F., Tissoux, H., 2021, Geometry of glaciofluvial
309 deposits and dynamics of the Lyonnais lobe ice front during the last glacial period
310 (France, Northern Alps): *Earth Science Bulletin BSGF*, *Accepted*
- 311 Sakawuchi, A.O., Blair, M.W., DeWitt, R., Faleiros, F.M., Hyppolito, T., and Guedes, C.C.F.,
312 2011, Thermal history versus sedimentary history: OSL sensitivity of quartz grains
313 extracted from rocks and sediments: *Quaternary Geochronology*, v. 6, p. 261–272,
314 <https://doi.org/10.1016/j.quageo.2010.11.002>
- 315 Seguinot, J., Ivy-Ochs, S., Jouvét, G., Huss, M., Funk, M., and Preusser, F., 2018, Modelling last
316 glacial cycle ice dynamics in the Alps: *The Cryosphere*, v. 12, p. 3265–3285,
317 <https://doi.org/10.5194/tc-12-3265>
- 318 Smedley, R.K., Glasser, N.F., and Duller, G.A.T., 2016, Luminescence dating of glacial
319 advances at Lago Buenos Aires (~46°S), Patagonia: *Quaternary Science Reviews*, v. 134,
320 p. 59–73, <http://dx.doi.org/10.1016/j.quascirev.2015.12.010>
- 321 Veres, D., Lallier-Vergès, E., Wohlfarth, B., Lacourse, T., Kéravis, D., Björck, S., Preusser, F.,
322 Andrieu-Ponel, V., and Ampel, L., 2009, Climate-driven changes in lake conditions
323 during late MIS 3 and MIS 2: a high-resolution geochemical record from Les Echets,
324 France: *Boreas*, v. 38, p. 230–243, <https://doi.org/10.1111/j.1502-3885.2008.00066.x>
- 325 Wirsig, C., Zasadni, J., Christl, M., Akçar, N., and Ivy-Ochs, S., 2016, Dating the onset of LGM
326 ice surface lowering in the High Alps: *Quaternary Science Reviews*, v. 143, p. 37–50,
327 <https://doi.org/10.1016/j.quascirev.2016.05.001>

328

329 **TABLE & FIGURE CAPTIONS**

330 Table 1: Sample locations and luminescence ages.

331 Figure 1: (a) Glacial geomorphology of the study area (Mandier, 1988; Roattino et al., 2021).
332 Inset: geomorphic limits of the LP ice maximum in the Alps (Ehlers et al., 2011) with main
333 LGM ice flows (light blue arrows; Wirsig et al., 2016), and location of the study area (black box)
334 with main ice-drainage catchments (dark blue limit, AR: Arve, IS: Isère). (b) Longitudinal
335 topographic profile (LP1) showing bedrock escarpement underlying the IMC ridges and
336 downstream glaciofluvial sediments (undifferentiated), when the glacier reached its LP
337 maximum extent. (c) Topographic cross-profile (ART site; CP1) showing the main three terrace
338 levels. The bedrock/sediment contact is extrapolated from borehole data (Roattino et al., 2021).

339

340 Figure 2: Quartz normal-like and feldspar (no fading correction) complex single-grain burial age
341 distributions for a representative sample (SPC5). Consistent quartz and feldspar sample burial
342 ages are obtained using the CAM and FMM models respectively, based on the different partial
343 bleaching diagnosis.

344

345 Figure 3: (a) Late Pleistocene Northern Alpine speleothems $\delta^{18}\text{O}$ (purple; Moseley et al., 2020)
346 and global marine sediments $\delta^{18}\text{O}$ (grey curve with MIS in shaded bars; Lisiecki and Raymo,
347 2005) records, with modelled Alpine ice volume (blue, GRIP paleoclimate forcing; Seguinot et
348 al., 2018). (b) Luminescence ages showing two main groups around MIS 4 (green) and late MIS
349 3 (orange), consistent with existing radiocarbon ages from the NW sector (green) and upstream
350 (red) of the IMC (Mandier et al., 2003). (c) Conceptual sketch illustrating the southward shift of
351 the North Atlantic storm track forced by gradual NH ice sheet growth (LGM extent in blue), with
352 impact on the paleo-atmospheric circulation (coloured arrows).

353

354 ¹GSA Data Repository item 201Xxxx, [Details of samples' geomorphological and
355 sedimentological context, and luminescence dating], is available online at
356 www.geosociety.org/pubs/ft20XX.htm, or on request from editing@geosociety.org.

Figure 1

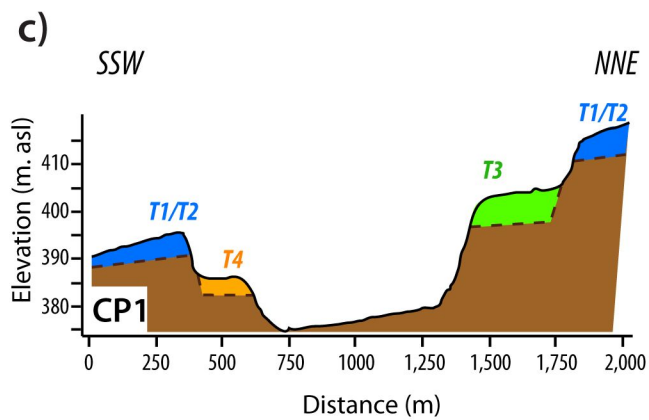
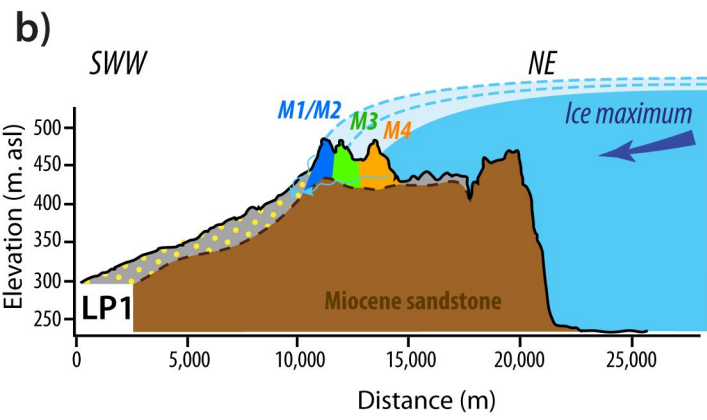
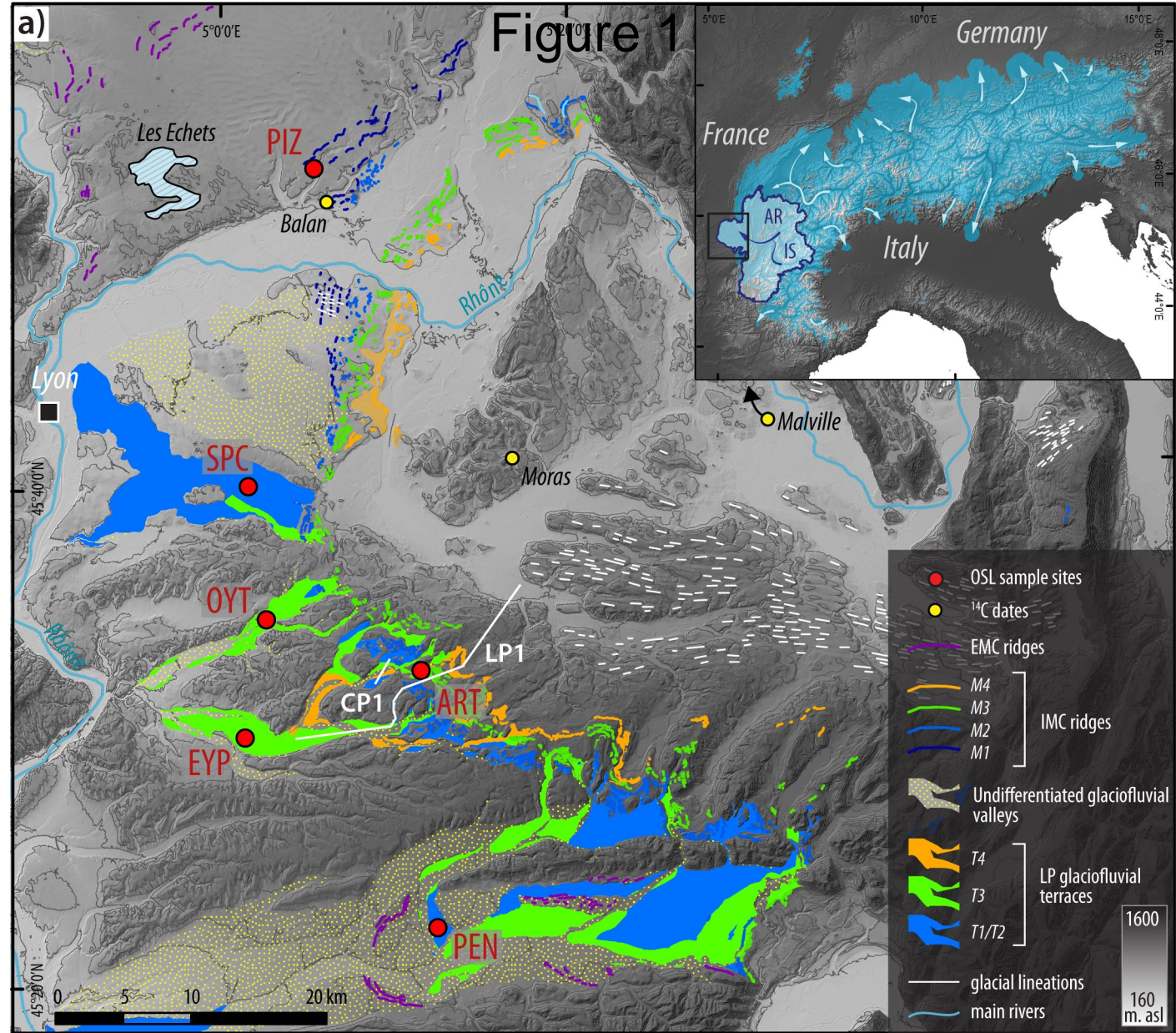
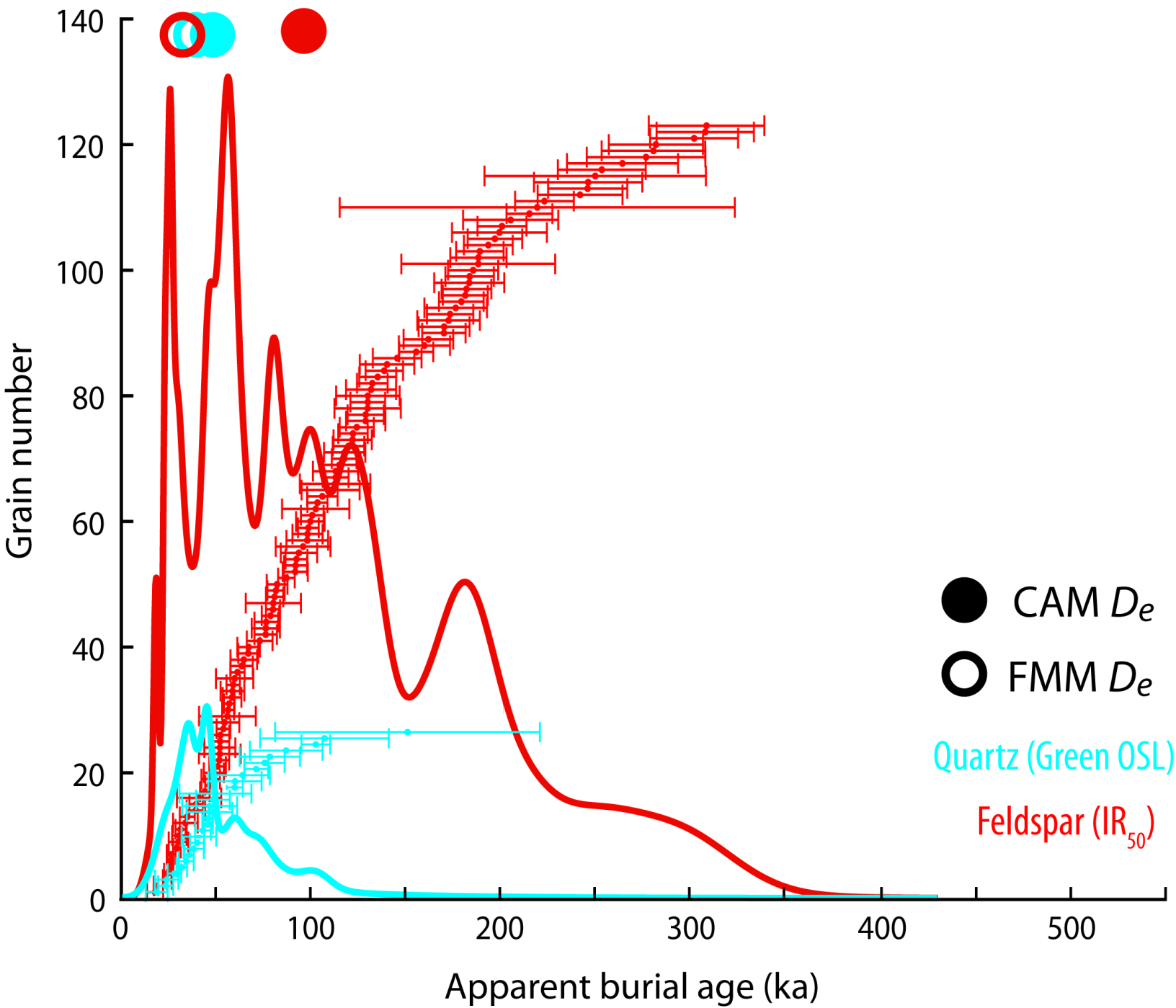
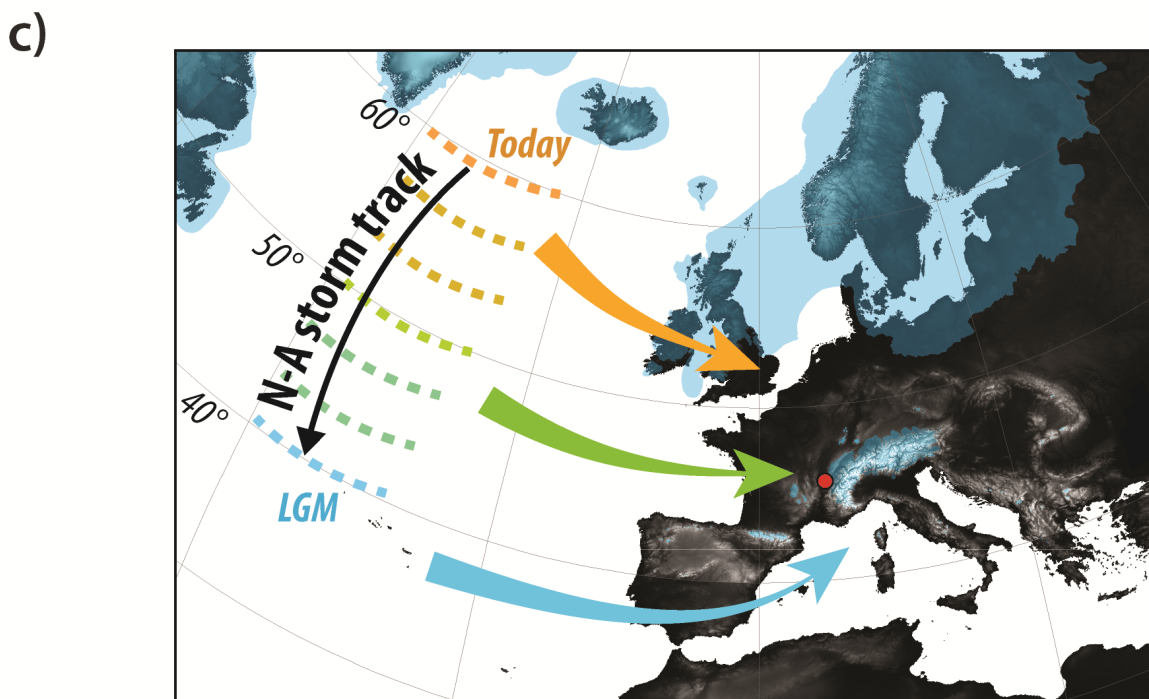
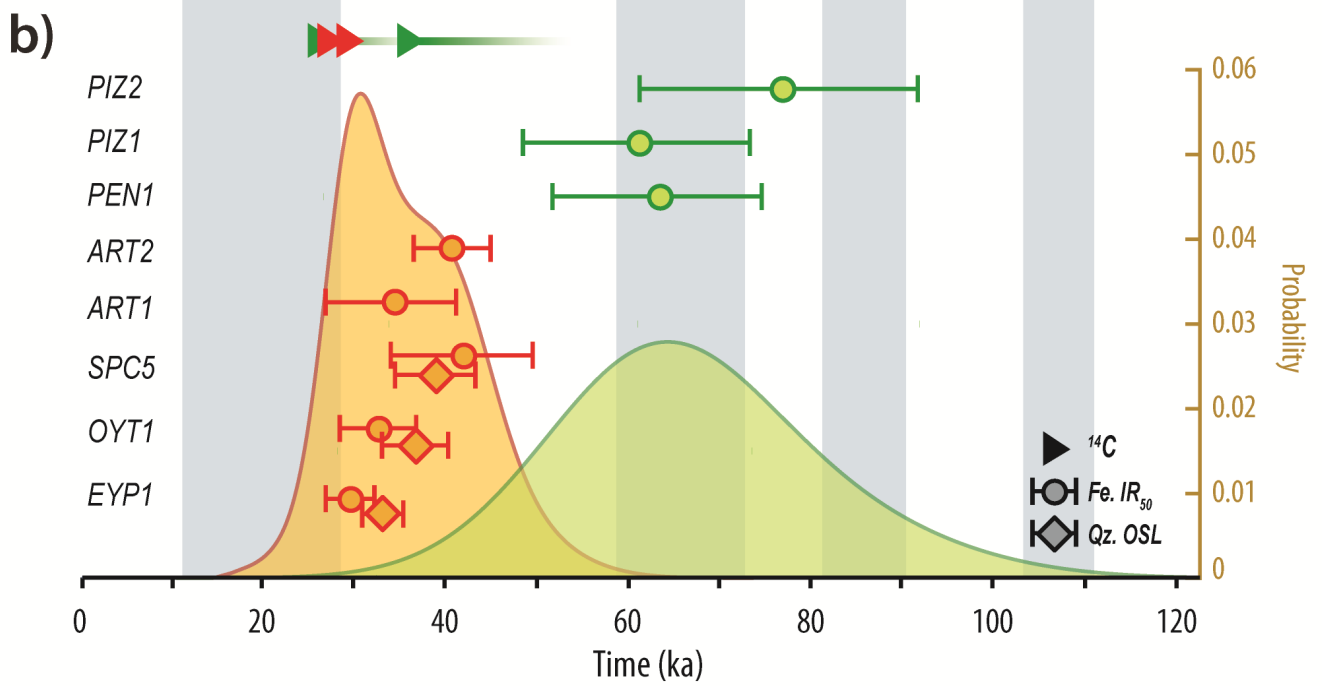
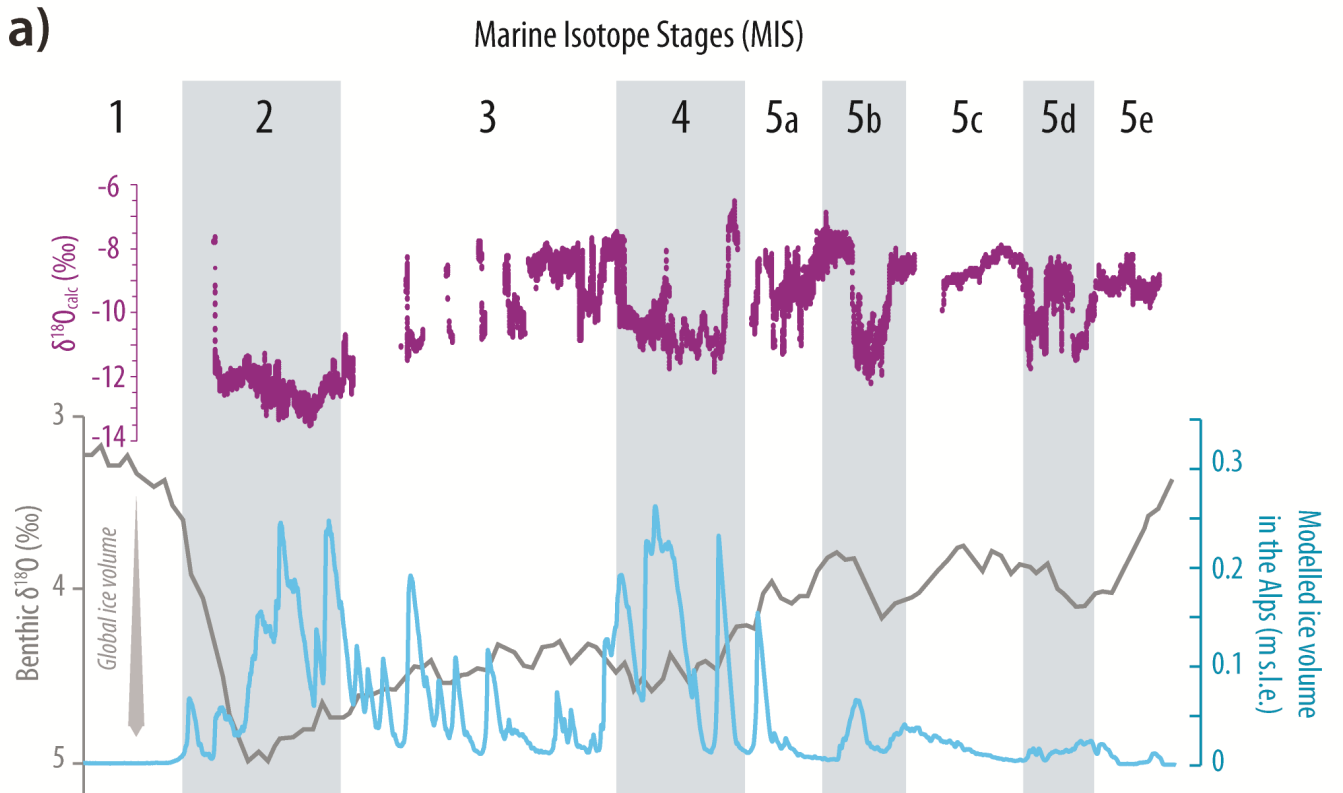


Figure 2





Gribenski et al., 2021—Table

Table 1. Sample locations and luminescence ages

Sample ID	Lat./ Long. (°N/°E)	Elevation (m a.s.l.)	Depth (m below surface)	Geomorphic unit	Quartz (OSL) age (ka)	Feldspar (IR ₅₀) age (ka)
EYP1	45.496/5.009	262	5	T3	32.9±2.3	29.4±2.8
OYT1	45.575/5.030	265	3.2	T3	36.4±3.8	32.4±4.3
SPC5	45.666/5.015	250	5	T1/T2	38.6±4.5	41.6±7.9
ART1	45.537/5.182	430	3	T4	-	33.8±7.3
ART2	45.536/5.182	420	12	T3 or T4	-	40.6±4.2
PEN1	45.363/5.186	313	12	T1/T2	-	63.0±11.4
PIZ1	45.876/5.088	250	13	underlying M1	-	60.8±12.3
PIZ2	45.876/5.088	256	2	underlying M1	-	76.4±15.1